LETTER

doi:10.1038/nature24019

Early trace of life from 3.95 Ga sedimentary rocks in Labrador, Canada

Takayuki Tashiro[1], Akizumi Ishida[2,3], Masako Hori[2,4], Motoko Igisu[5], Mizuho Koike[2], Pauline Méjean[2], Naoto Takahata[2], Yuji Sano[2]§ & Tsuyoshi Komiya[1]§

The vestiges of life in Eoarchean rocks have the potential to elucidate the origin of life. However, gathering evidence from many terrains is not always possible[1–3], and biogenic graphite has thus far been found only in the 3.7–3.8 Ga (gigayears ago) Isua supracrustal belt[4–7]. Here we present the total organic carbon contents and carbon isotope values of graphite ($\delta^{13}C_{org}$) and carbonate ($\delta^{13}C_{carb}$) in the oldest metasedimentary rocks from northern Labrador[8,9]. Some pelitic rocks have low $\delta^{13}C_{org}$ values of −28.2, comparable to the lowest value in younger rocks. The consistency between crystallization temperatures of the graphite and metamorphic temperature of the host rocks establishes that the graphite does not originate from later contamination. A clear correlation between the $\delta^{13}C_{org}$ values and metamorphic grade indicates that variations in the $\delta^{13}C_{org}$ values are due to metamorphism, and that the pre-metamorphic value was lower than the minimum value. We concluded that the large fractionation between the $\delta^{13}C_{carb}$ and $\delta^{13}C_{org}$ values, up to 25‰, indicates the oldest evidence of organisms greater than 3.95 Ga. The discovery of the biogenic graphite enables geochemical study of the biogenic materials themselves, and will provide insight into early life not only on Earth but also on other planets.

The presence of life on early Earth is still controversial owing to the scarcity and poor preservation of the Eoarchean records. Isotopic compositions of graphite in the Eoarchean sedimentary rocks in the Isua supracrustal belt (ISB) suggest that the graphite grains have biogenic origins because of the enrichment of light carbon isotope[4–7]. However, biogenic graphite has not been discovered in the 3.83 Ga Akilia association and 3.75 Ga Nuvvuagittuq supracrustal belt[1–3]. Recent reassessment of uranium–lead (U–Pb) dating and cathodoluminescence observation of zircons from the Uivak Gneiss in Saglek Block (Fig. 1), northern Labrador, Canada indicated the presence of the oldest supracrustal rock in the world, intruded by the more than 3.95 Ga Uivak-Iqaluk Gneiss[8,9]. Here we report for the first time, to our knowledge, on the occurrence and geochemical characteristics of the oldest graphite.

We found graphite from the oldest metasedimentary rocks, including pelitic rocks, conglomerates, carbonate rocks, and chert nodules in the carbonate rocks from five areas of different metamorphic grades in the Saglek Block (Fig. 1). We obtained concentrations and isotopic compositions of the graphite using a graphite combustion method with an elemental analyser (vario MICRO cube, Elementar) connected to a mass spectrometer (IsoPrime100, Isoprime)[10]. We also performed *in situ* analyses of their carbon isotope ratios using a NanoSIMS 50 instrument. The results are presented as $\delta^{13}C$ values relative to a VPDB (Vienna Pee Dee Belemnite) standard.

Pelitic rocks occur ubiquitously in the Saglek block and often have preserved bedding planes (Extended Data Figs 1, 2). The graphite grains occur as aggregates and elongated shapes (up to a few tens to hundreds μm long) mostly along grain boundaries of other minerals, parallel to the bedding planes (Extended Data Fig. 2e, f). Some are enclosed within quartz, garnet, and biotite to form small globular shapes. The occurrence of graphite is analogous to the Phanerozoic organic matter with laminated morphology[11]. The pelitic rocks have large variations between 0.02 and 0.62 wt% in total organic carbon (TOC) contents and between −28.2 and −11.0‰ in $\delta^{13}C_{org}$ values, respectively (Extended Data Table 1), and show a negative correlation between them (Fig. 2). Graphite grains in a pelitic rock (LAF491) at St. John's Harbour South showed $\delta^{13}C_{org}$ values between −19.3 and −30.8‰ (Extended Data Table 2), which were consistent with the whole-rock carbon isotope value (Extended Data Fig. 3a).

Conglomerates at St. John's Harbour East contain pebble- to boulder-sized quartzite clasts (Extended Data Fig. 2b). Most of the graphite grains are elongated (up to a few tens μm long) or form aggregates along the bedding planes. Some graphite grains also occur as small globular inclusions of 1–2 μm, in the quartz, garnet, biotite, plagioclase, and amphibole grains. The TOC contents of the matrices are relatively low (~0.07 wt%) and the $\delta^{13}C_{org}$ values range between −27.6 and −20.8‰ (Fig. 2).

Carbonate rocks are also found in St. John's Harbour East, and have some chert nodules (Extended Data Fig. 2c). Graphite grains form elongated shapes or aggregates of globules. The carbonate rocks have distinctive positive La, Eu, and Y anomalies on the shale-normalized rare earth element patterns, diagnostic of chemical sediments, precipitated from seawater mixed with hydrothermal fluid (Extended Data Fig. 3b). The TOC contents of carbonate rocks range between 0.09 and 0.16 wt%, and the $\delta^{13}C_{org}$ and $\delta^{13}C_{carb}$ values are between −6.9 and −9.9‰ and between −3.8 and −2.6‰, respectively (Extended Data Table 1, Fig. 2). It is well known that the $\delta^{13}C_{carb}$ value decreases with later alteration[7] so that a $\delta^{13}C$ value of marine inorganic carbon in the Eoarchean is estimated to be higher than the maximum value (−2.6‰). The graphite grains in the chert nodules form globular shapes, ranging from between 1 and 100 μm across, and occur along grain boundaries or as inclusions within quartz grains (Extended Data Fig. 2h). The graphite grains range between −26.1 and −33.6‰ in $\delta^{13}C_{org}$ values (Extended Data Table 2), whereas the TOC contents and $\delta^{13}C_{org}$ values of the host rock are around 0.02 wt% and −10‰, respectively (Fig. 2). No graphite was recognized in the Pangertok Inlet and cherts in all the areas. In the St. John's Harbour East area, the $\delta^{13}C_{org}$ values are apparently dependent on the lithology, and increase in order from conglomerate through pelitic rocks to carbonate rocks and chert nodules (Fig. 2). The lithology-dependent variation of the $\delta^{13}C_{org}$ values suggests that the organic matter is autochthonous.

Metamorphic temperatures of host rocks with graphite grains were estimated via two methods: conventional mineral parageneses of ambient metabasites and geothermometry of garnet–biotite pairs in pelitic rocks. The metabasites in St. John's Harbour South, St. John's Harbour East, and Big Island have mineral parageneses of hornblende, plagioclase, and titanite, whereas those in Shuldham Island have a

[1]Department of Earth Science and Astronomy, Graduate School of Arts and Sciences, The University of Tokyo, Tokyo 153-8902, Japan. [2]Atmosphere and Ocean Research Institute, The University of Tokyo, Chiba 277-8564, Japan. [3]Institute for Excellence in Higher Education, Tohoku University, Sendai 9808576, Japan. [4]Department of Arts and Sciences, Osaka Kyoiku University, Osaka 582-8582, Japan. [5]Laboratory of Ocean-Earth Life Evolution Research, Japan Agency for Marine-Earth Science and Technology (JAMSTEC), Kanagawa 237-0061, Japan.
§These authors jointly supervised this work.

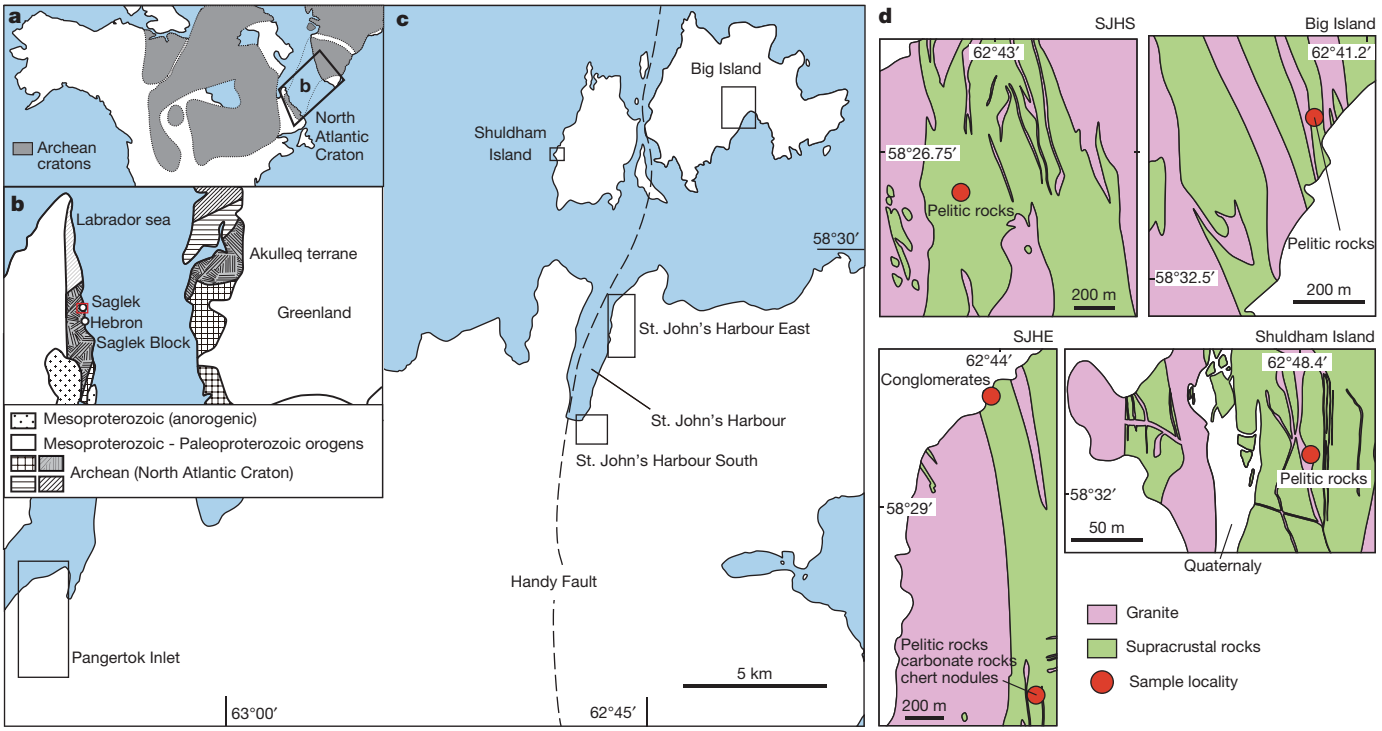

Figure 1 | Geological maps and sample localities in Saglek Block. **a**, Distribution of the Archean cratons, and Saglek Block is the western part of the North Atlantic Craton. **b**, Distribution of the Archean terrains in the western part of the North Atlantic Craton. The Saglek Block is equivalent to the Akulleq terrane in West Greenland. **c**, Northeastern part of the Saglek Block, showing our five studied areas. **d**, Localities of the graphite-bearing samples in the studied areas.

mineral paragenesis of clinopyroxene, hornblende, and plagioclase. The metamorphic temperatures of St. John's Harbour South, St. John's Harbour East, Big Island, and Shuldham Island were estimated from chemical compositions of garnet and biotite as 653 ± 16 (1σ) °C, 691 ± 26 °C, 585 ± 45 °C and 700 to 800 °C, respectively (Extended Data Table 3).

We also estimated crystallization temperatures of graphite on the basis of Raman spectra of graphite[12,13] with confocal laser Raman microspectroscopy. It was found that the crystallization temperatures of graphite are over 563 ± 50 °C for the pelitic rocks, conglomerates, and carbonate rocks, and between 536 ± 50 and 622 ± 50 °C for the chert nodules (Extended Data Table 4). The estimated crystallization temperatures of graphite are mostly consistent with the metamorphic temperature of the host rocks, except for chert nodules (Extended Data Fig. 4). The metamorphic history of the Saglek Block is complex, and some major metamorphisms were estimated through dating of the zircons of the Uivak-Iqaluk Gneisses[9]. The first metamorphic episode was estimated to have occurred around 3.89 Ga owing to the intrusion of a younger suite of Uivak Gneisses. The second episode occurred 3.6 Ga owing to the intrusion of Uivak II gneiss[14], and the third 2.7 Ga from U–Pb dating of zircon overgrowths[9,15] and secondary isochrons of the Uivak Gneiss[16]. The discontinuous intrusions of many generations of granitoid at least around 3.95, 3.87, 3.6 and 3.3 Ga[9,14,17,18] and lack of basal conglomerates indicate that the supracrustal rocks have settled throughout in a deep crust so that later contamination of sedimentary graphite grains would have been impossible from 3.9 to 3.3 Ga. The lines of evidence of the occurrence of graphite parallel to the bedding planes, consistency between the Raman spectra and metamorphic temperature, lithology-dependent $\delta^{13}C_{org}$ variation and discontinuous metamorphic and magmatic ages suggest that the graphite has a sedimentary origin that predates the first metamorphic episode.

The maximum $\delta^{13}C_{org}$ values of pelitic rocks increase between −18.1 and −11.0‰ with an increasing metamorphic grade from amphibolite facies to granulite facies (Fig. 3). The good correlation indicates that the variations of $\delta^{13}C_{org}$ values were due to later metamorphism so that the pre-metamorphic $\delta^{13}C_{org}$ value was lower than the minimum $\delta^{13}C_{org}$ values of −28.2‰. The low $\delta^{13}C_{org}$ values of pelitic rocks and conglomerates are consistent with the biotic origin of graphite. However, it is well known that ^{13}C-depleted graphite could be produced by abiotic processes including high temperature disproportionation

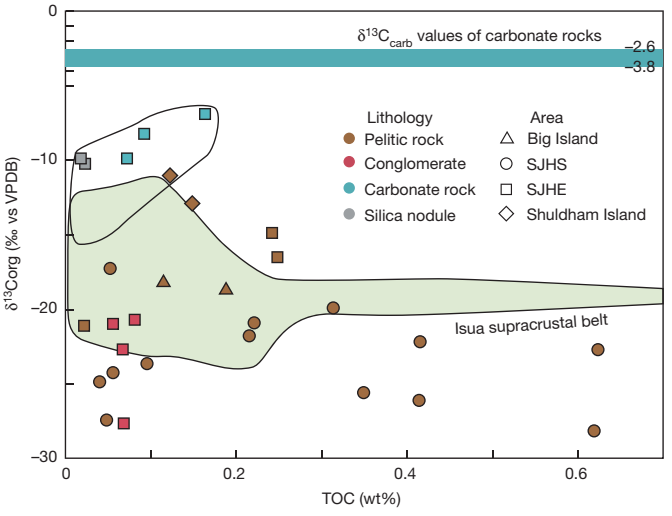

Figure 2 | Correlation between TOC contents and $\delta^{13}C_{org}$ values. We analysed the whole-rock TOC contents and carbon isotopes of 20 pelitic rocks, four conglomerates, three carbonate rocks and two chert nodules in carbonate rocks. The carbonate rocks and silica nodules in the carbonate rocks have relatively higher $\delta^{13}C_{org}$ values whereas the $\delta^{13}C_{org}$ values of matrices of the conglomerates are much lower. The TOC contents and the $\delta^{13}C_{org}$ values of the pelitic rocks have large variations and display a negative correlation. Analytical errors are smaller than symbols. No statistical methods were used to predetermine sample size. The experiments were not randomized and the investigators were not blinded to allocation during experiments and outcome assessment.

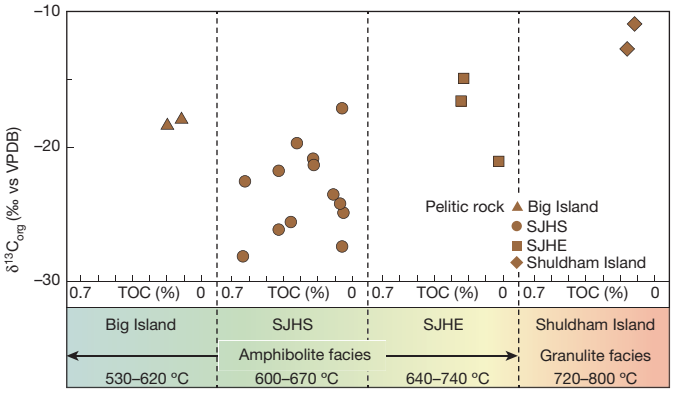

Figure 3 | Comparison between the $\delta^{13}C_{org}$ values of pelitic rocks and metamorphic grades. Metamorphic grades are estimated from mineral parageneses of the surrounding metabasalts and garnet–biotite geothermometry of the graphite-bearing pelitic rocks. The $^{13}C_{org}$ values are positively correlated with the metamorphic grades. Analytical errors are smaller than symbols.

of siderite[19,20], low temperature Fischer–Tropsch-type synthesis[21] and incorporation of meteoritic organic matter[7]. The disproportionation of the siderite can be represented by the following reaction[19]: $6FeCO_3 \rightarrow 2Fe_3O_4 + 5CO_2 + C$, which occurs at temperatures above 450 °C for pure siderite. However, the graphite in clastic sedimentary rocks is inconsistent with siderite decomposition because they contain neither siderite nor magnetite. On the other hand, the siderite decomposition pathway cannot be excluded for the carbonate rocks because they contain magnetite, and the isotopic differences, 4 to 6‰, between graphite and carbonate ($\delta^{13}C_{carb}$–$\delta^{13}C_{org}$) in the carbonate rocks are consistent with equilibrium isotopic fractionation during graphite formation from siderite at around 700 °C[20]. The Fischer–Tropsch-type synthesis requires an appropriate catalyst such as Ni-Fe metal and magnetite, and a source of H_2 and CO, and the reaction is operated between 200 and 350 °C[21,22]. Although the H_2-rich reducing conditions can be produced by hydrothermal alternation of ultramafic rocks[21,22], the highly ^{13}C-depleted graphite grains are present only in the clastic sedimentary rocks without ultramafic rock-derived chromite, hence the contribution of the Fischer–Tropsch-type synthesis is insignificant.

We conclude that the graphite from clastic sedimentary rocks in the Saglek Block has a biogenic origin and the primary $\delta^{13}C_{org}$ and $\delta^{13}C_{carb}$ values were estimated to be less than −28.2 and greater than −2.6‰, respectively. As a result, the isotopic fractionation between graphite and carbonate ($\delta^{13}C_{carb}$–$\delta^{13}C_{org}$) reached −25.6‰ more than those in turbidite-derived sedimentary rocks of the Isua supracrustal belt[6]. The large fractionation provides the oldest evidence for autotrophs, using the reductive acetyl-CoA pathway or the Calvin cycle, over 3.95 Ga (Extended Data Fig. 5).

Online Content Methods, along with any additional Extended Data display items and Source Data, are available in the online version of the paper; references unique to these sections appear only in the online paper.

Received 14 February; accepted 21 August 2017.

1. Fedo, C. M. & Whitehouse, M. J. Metasomatic origin of quartz-pyroxene rock, Akilia, Greenland, and implications for Earth's earliest life. *Science* **296,** 1448–1452 (2002).
2. Papineau, D. *et al.* Young poorly crystalline graphite in the >3.8-Gyr-old Nuvvuagittuq banded iron formation. *Nat. Geosci.* **4,** 376–379 (2011).
3. Sano, Y., Terada, K., Takahashi, Y. & Nutman, A. P. Origin of life from apatite dating? *Nature* **400,** 127–128 (1999).
4. Hayes, J. M., Kaplan, I. R. & Wedeking, K. W. in *Earth's Earliest Biosphere: Its Origin and Evolution* (ed. Schopf, J.W.), 93–134 (Princeton University Press, 1983).
5. Ohtomo, Y., Kakegawa, T., Ishida, A., Nagase, T. & Rosing, M. T. Evidence for biogenic graphite in early Archaean Isua metasedimentary rocks. *Nat. Geosci.* **7,** 25–28 (2014).
6. Rosing, M. T. ^{13}C-Depleted carbon microparticles in >3700-Ma sea-floor sedimentary rocks from west greenland. *Science* **283,** 674–676 (1999).
7. Schidlowski, M., Appel, P. W. U., Eichmann, R. & Junge, C. E. Carbon isotope geochemistry of the 3.7 x 10^9-yr-old Isua sediments, West Greenland: implications for the Archaean carbon and oxygen cycles. *Geochim. Cosmochim. Acta* **43,** 189–199 (1979).
8. Komiya, T. *et al.* Geology of the Eoarchean, >3.95 Ga, Nulliak supracrustal rocks in the Saglek Block, northern Labrador, Canada: The oldest geological evidence for plate tectonics. *Tectonophysics* **662,** 40–66 (2015).
9. Shimojo, M. *et al.* Occurrence and geochronology of the Eoarchean, ~3.9 Ga, Iqaluk Gneiss in the Saglek Block, northern Labrador, Canada: Evidence for the oldest supracrustal rocks in the world. *Precambr. Res.* **278,** 218–243 (2016).
10. Vandenbroucke, M. Kerogen: from types to models of chemical structure. *Oil & Gas Science and Technology - Rev. IFP* **58,** 243–269 (2003).
11. Vandenbroucke, M. & Largeau, C. Kerogen origin, evolution and structure. *Org. Geochem.* **38,** 719–833 (2007).
12. Beyssac, O., Goffé, B., Chopin, C. & Rouzaud, J. N. Raman spectra of carbonaceous material in metasediments: a new geothermometer. *J. Metamorph. Geol.* **20,** 859–871 (2002).
13. Igisu, M. *et al.* FTIR microspectroscopy of Ediacaran phosphatized microfossils from the Doushantuo Formation, Weng'an, South China. *Gondwana Res.* **25,** 1120–1138 (2014).
14. Collerson, K. D. & Bridgwater, D. in *Trondhjemites, Dacites, and Related Rock* (ed. Barker, F.) (Elsevier, 1979).
15. Nutman, A. P. & Collerson, K. D. Very early Archean crustal-accretion complexes preserved in the North Atlantic craton. *Geology* **19,** 791–794 (1991).
16. Collerson, K. D. The Archean gneiss complex of northern Labrador. 2. Mineral ages, secondary isochrons, and diffusion of strontium during polymetamorphism of the Uivak gneisses. *Can. J. Earth Sci.* **20,** 707–718 (1983a).
17. Schiøtte, L., Compston, W. & Bridgwater, D. U–Th–Pb ages of single zircons in Archaean supracrustals from Nain Province, Labrador, Canada. *Can. J. Earth Sci.* **26,** 2636–2644 (1989).
18. Komiya, T. *et al.* A prolonged granitoid formation in Saglek Block, Labrador: Zonal growth and crustal reworking of continental crust in the Eoarchean. *Geoscience Frontiers* (in the press) (2016).
19. Perry, E. C. & Ahmad, S. N. Carbon isotope composition of graphite and carbonate minerals from 3.8-AE metamorphosed sediments, Isukasia, Greenland. *Earth Planet. Sci. Lett.* **36,** 280–284 (1977).
20. van Zuilen, M. A. *et al.* Graphite and carbonates in the 3.8 Ga old Isua Supracrustal Belt, southern West Greenland. *Precambr. Res.* **126,** 331–348 (2003).
21. Horita, J. Some perspectives on isotope biosignatures for early life. *Chem. Geol.* **218,** 171–186 (2005).
22. De Gregorio, B., Sharp, T., Rushdi, A. & Simoneit, B. T. in *Earliest Life on Earth: Habitats, Environments and Methods of Detection* (eds Golding, S. D. & Glikson, M.), 239–289 (Springer, 2011).

Supplementary Information is available in the online version of the paper.

Acknowledgements This research was supported by the Ministry of Education, Culture, Sports, Science and Technology, Japan (grant numbers: 23253007, 26220713 and 24221002) and the Mitsubishi Foundation. We thank K. D. Collerson and B. Ryan for sharing their geological information. We are grateful to W. Broomfield, Parks Canada, Labrador Inuit Development Corporation (LIDC) and many bear monitors who assisted with our geological fieldwork at the Saglek Block.

Author Contributions T.K. designed the study and Y.S. designed the geochemical study. T.K., T.T., A.I., M.H., M.I., M.K., P.M., N. T., and Y.S. conducted geochemical analyses. T.K. and T.T. collected samples in the field. T.K. wrote the manuscript with important contributions from all co-authors.

Author Information Reprints and permissions information is available at www.nature.com/reprints. The authors declare no competing financial interests. Readers are welcome to comment on the online version of the paper. Publisher's note: Springer Nature remains neutral with regard to jurisdictional claims in published maps and institutional affiliations. Correspondence and requests for materials should be addressed to T.K. (komiya@ea.c.u-tokyo.ac.jp) or Y.S. (ysano@aori.u-tokyo.ac.jp).

Reviewer Information *Nature* thanks A. Polat and the other anonymous reviewer(s) for their contribution to the peer review of this work.

METHODS

Extraction and isotope analysis of organic carbon. We collected 156 sedimentary rocks from the Saglek area, and found graphite in 54 rock samples. We selected 28 samples with a larger amount of the graphite to cover all of lithologies and studied areas for geochemical works. The powdered rock samples were prepared by crushing rock chips. They (1–3 g) were decarbonated by 6 N HCl at 70 °C for 12 h. The HCl treated samples were further treated with mixed acid of HCl, HF and H_2O (1:4:4 v/v/v in 10 N HCl) at 60 °C for 3 days and repeated 3–4 times, followed by 6 N HCl at 70 °C for 12 h in order to eliminate the remaining elements which are able to form complex fluorides such as ralstonite ($Na_xMg_xAl_{2-x}(FOH)_6H_2O$) upon drying[10]. All acid reactions were performed in shaking bath to facilitate acid attacks. The acid-treated samples were finally washed with pure water several times and freeze-dried. The HCl–HF-treated sample powders were placed in an Sn capsule in the range of 1–40 mg and 30–500 μg, respectively, and were combusted with oxygen under He career flow at 1,100 °C in an elemental analyser (vario MICRO cube, Elementar) connected to mass spectrometer (IsoPrime100, Isoprime), housed at Atmosphere and Ocean Research Institute, The University of Tokyo in order to measure carbon concentration and isotope composition, respectively. Carbon, nitrogen, and sulphur in samples were converted into CO_2, N_2, and SO_2, respectively. Carbon concentrations and isotope compositions of samples were calibrated against an in-house standard material (sulfanilamide), whose carbon concentration and isotope composition were known (41.81 wt%C, $\delta^{13}C = -26.6‰$). Based on the replicate analyses of the in-house standard material, analytical reproducibility is within ± 0.5‰ (2σ). Results were reported as $\delta^{13}C$ values relative to a VPDB standard.

Carbon isotopes of carbonate. Powdered samples were prepared from several parts of fresh-cut surfaces of rock samples using a micro-drill with a 3-mm-diameter bit. They were analysed with a Finnigan MAT Delta Plus mass spectrometer interfaced with a Gas Bench II, housed at Atmosphere and Ocean Research Institute, The University of Tokyo. The samples were reacted with purified H_3PO_4 at 70 °C in a glass vial preliminary filled with He gas. The results were reported in ‰ relative to VPDB using the NBS18 standard ($\delta^{13}C = -5.014‰$). The analytical reproducibility is within ± 0.2‰ (2σ).

***In situ* carbon isotope analyses of individual graphite grains.** We conducted in-situ analyses of carbon isotope values of individual graphite grains with a NanoSIMS 50 instrument installed at the Atmosphere and Ocean Research Institute. Prior to the carbon isotope analyses, carbon coating on thin sections was completely removed by re-polishing. The samples were then gold coated and baked at around 100 °C in the NanoSIMS air-lock for a week. An around 2-pA Cs^+ primary beam with a beam diameter of less than 0.6 μm was rastered over $5 \times 5\,\mu m^2$ square areas of the graphite gains in the sections. Each analysed area was pre-sputtered with a 200-pA primary beam over the larger raster area ($10 \times 10\,\mu m^2$) for 240 s. We used two magnetic fields with the NanoSIMS multi-collection system: In the magnetic field 1 (B1), secondary ions of $^{12}C^-$ and $^{12}C^{12}C^-$ were detected by electron multiplier EM4 and EM5, with counting time of 3 s. Then, the magnetic field was cycled to the second mass (B2). Secondary ions of $^{12}C^-$, $^{13}C^-$, and $^{12}C^{14}N^-$ were detected simultaneously by EM3, EM4, and EM5, respectively. The counting time for B2 was 20 s. A total of 25 cycles is required for 1 measurement, corresponding to the total counting time of 75 s for B1 and 500 s for B2, respectively. The carbon isotopic ratios $(^{13}C/^{12}C)_{EM4}$ were calculated from $^{12}C^-$ in B1 and $^{13}C^-$ in B2, using the single detector (EM4). The multi-collection $(^{13}C/^{12}C)_{multi}$ ratios, which used the simultaneous collection of two detectors (EM3 and EM4 in B2), were also calculated and compared to the $(^{13}C/^{12}C)_{EM4}$ ratios, to check the stability of the measurement. During the analyses, $^{12}C^{12}C^-/^{12}C^-$ and $^{12}C^{14}N^-/^{12}C^-$ ratios were monitored to check potential contamination. The carbon isotope compositions were calibrated against an in-house standard material (artificial pure graphite). Its carbon isotope composition was determined as $\delta^{13}C = -26.6‰$, using the conventional method with the IsoPrime 100 analytical system. Based on the replicate analyses of the standard, analytical reproducibility of NanoSIMS 50 is within ±3‰ (1σ).

Major and trace element analysis of carbonate rocks. We analysed major element and rare earth element compositions of carbonate rocks to determine their origin. The major element compositions were analysed with X-ray fluorescence spectrometry (XRF: RIGAKU RIX-2100) at the Tokyo Institute of Technology using fused glass beads. The rare earth elements were analysed by inductively coupled plasma mass spectrometry (ICP–MS: Agilent 7500 s) at Komaba, the University of Tokyo. The analytical methods were described elsewhere[23].

Mineral compositions and garnet–biotite geothermometry. We analysed mineral compositions of garnet and biotite in the pelitic rocks and employed garnet–biotite geothermometry[24] to estimate metamorphic temperature. Back-scattered electron images of all the thin sections of pelitic rocks and chemical compositions of minerals were obtained with an electron probe microanalyzer (JEOL-JXA-8800) at The University of Tokyo. All analyses were performed with an accelerating voltage of 15 kV, 12 nA beam current and a counting time of 10–40 s. The oxide ZAF correction method was applied. The analyses were performed on adjacent grains and across the grain boundaries in order to check compositional zonation for each mineral.

Raman microspectroscopy. A laser Raman micro-spectrometer (JASCO NRS-2000) was used to estimate metamorphic temperature of the graphite. The thin sections were twice exposed to an Ar laser (514.5 nm) for 60 to 80 s at a laser power of about 5 mW at the sample surface to obtain Raman spectra in the range of 1,800 to 1,100 cm^{-1} at 1 cm^{-1} resolution. 100× (NA, 0.84) and 50× (NA, 0.80) objective lenses were used, so the spatial resolution of the Raman analysis was about 1–2 μm. We only analysed the graphite embedded within the rocks below the surface of the thin section in order to avoid the effect of polishing, which can induce deformation of carbonaceous matter during sample preparation and thus possibly induce artificial modification of the Raman spectroscopic feature[25]. Details of the analytical methods are described elsewhere[12,13]. A Raman spectrum of graphite is composed of first-order and second-order regions, and the first-order region from 1,100 to 1,800 cm^{-1} is often considered[26,27]. In this region, a graphite band (G band) occurs at around 1,580 cm^{-1}, whereas poorly ordered carbon displays D1 (~1,350 cm^{-1}), D2 (~1,620 cm^{-1}) and D3 bands (~1,500 cm^{-1}), respectively. The crystallization temperature can be estimated using following spectral parameters[12]:

$$T(°C) = -455 \times D1/(G + D1 + D2)\text{band area ratio} + 641$$

This equation works in the temperature range of 330 to 650 °C and the error is estimated at ± 50 °C[12]. Peak position, band-area (that is, integrated area) and band-width (that is, full width at half maximum, FWHM) were determined using a computer program PeakFit 4.12 (SeaSolve Software Inc.).

Data availability. The data that support the findings of this study are available from the corresponding author upon reasonable request. The rock samples are stored at The University of Tokyo.

23. Koshida, K., Ishikawa, A., Iwamori, H. & Komiya, T. Petrology and geochemistry of mafic rocks in the Acasta Gneiss Complex: Implications for the oldest mafic rocks and their origin. *Precambr. Res.* **283,** 190–207 (2016).
24. Ferry, J. M. & Spear, F. S. Experimental calibration of the partitioning of Fe and Mg between biotite and garnet. *Contrib. Mineral. Petrol.* **66,** 113–117 (1978).
25. Pasteris, J. D. *In situ* analysis in geological thin-sections by laser raman microprobe spectroscopy: A cautionary note. *Appl. Spectrosc.* **43,** 567–570 (1989).
26. Nemanich, R. J. & Solin, S. A. First- and second-order Raman scattering from finite-size crystals of graphite. *Phys. Rev. B* **20,** 392–401 (1979).
27. Tuinstra, F. & Koenig, J. L. Raman spectrum of graphite. *J. Chem. Phys.* **53,** 1126–1130 (1970).
28. Hayes, J. M., Kaplan, I. R. & Wedeking, K. W. in *Earth's Earliest Biosphere: Its Origin and Evolution* (ed. Schopf, J.W.) 93–134 (Princeton Univ. Press, 1983).
29. Naraoka, H., Ohtake, M., Maruyama, S. & Ohmoto, H. Non-biogenic graphite in 3.8-Ga metamorphic rocks from the Isua district, Greenland. *Chem. Geol.* **133,** 251–260 (1996).
30. Oehler, D. Z. & Smith, J. W. Isotopic composition of reduced and oxidized carbon in early Archaean rocks from Isua, *Greenland. Precamb. Res.* **5,** 221–228 (1977).
31. Ohtomo, Y., Kakegawa, T., Ishida, A., Nagase, T. & Rosing, M. T. Evidence for biogenic graphite in early Archaean Isua metasedimentary rocks. *Nat. Geosci.* **7,** 25–28 (2014).
32. Perry, E. C. & Ahmad, S. N. Carbon isotope composition of graphite and carbonate minerals from 3.8-AE metamorphosed sediments, Isukasia, Greenland. *Earth Planet. Sci. Lett.* **36,** 280–284 (1977).
33. Rosing, M. T. ^{13}C-depleted carbon microparticles in > 3700-Ma sea-floor sedimentary rocks from West Greenland. *Science* **283,** 674–676 (1999).
34. Schidlowski, M., Appel, P. W. U., Eichmann, R. & Junge, C. E. Carbon isotope geochemistry of the 3.7 x 10^9-yr-old Isua sediments, West Greenland: implications for the Archaean carbon and oxygen cycles. *Geochim. Cosmochim. Acta* **43,** 189–199 (1979).
35. Shimoyama, A. & Matsubaya, O. Carbon isotope compositions of graphite and carbonate in 3.8×10^9 years old Isua rocks. *Chem. Lett.* **7,** 1205–1208 (1992).
36. Ueno, Y., Isozaki, Y., Yurimoto, H. & Maruyama, S. Carbon isotopic signatures of individual Archean microfossil (?) from Western Australia. *Intl Geol. Rev.* **43,** 196–212 (2001).

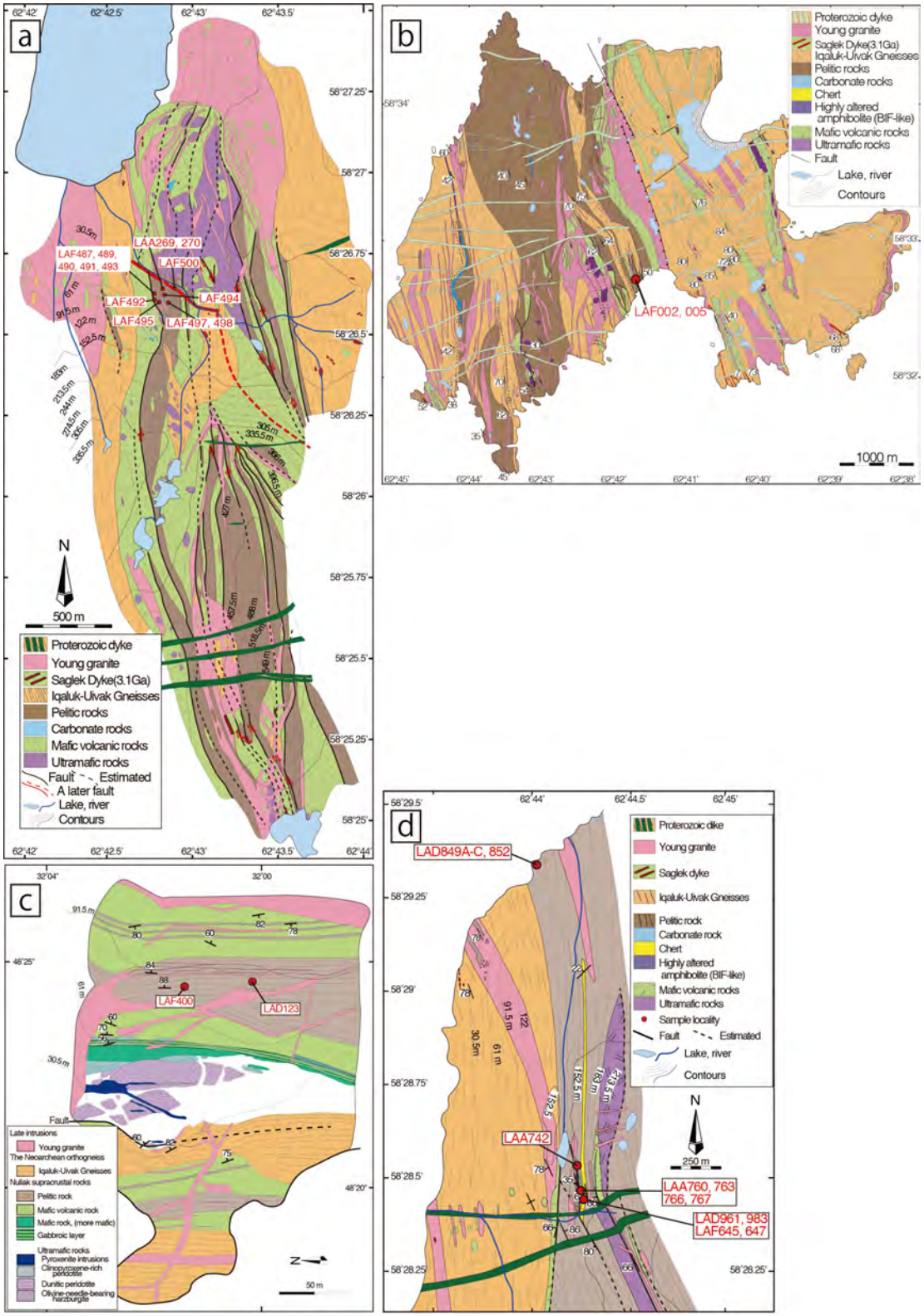

Extended Data Figure 1 | Detailed geological maps of four areas in the Saglek Block. a, A geological map of St. John's Harbour South area (SJHS). The area is composed of the supracrustal rocks, Iqaluk-Uivak Gneisses, Saglek dykes, young granite intrusion and the Proterozoic mafic dikes. The supracrustal rocks form a NS-trending belt, and are intruded by around 3.95 Ga Iqaluk-Uivak Gneisses. The pelitic rocks are predominant in the supracrustal rocks. **b**, A geological map of Big Island area. The area is subdivided into two parts by a NS-trending fault. The eastern side is composed of the supracrustal rocks, Iqaluk-Uivak Gneisses, Saglek dykes, young granite intrusion and the Proterozoic mafic dykes. The western side is predominant in pelitic rocks, and contains ultramafic and mafic rocks, and carbonate rocks. **c**, A geological map of a small point of the western coast of the Shuldham Island. The area is characterized by ultramafic rocks with large olivine-needle structures. The ultramafic rock-bearing body consists of harzburgitic ultramafic rocks, olivine-clinopyroxene rocks, clinopyroxene-hornblendite, gabbroic rocks, fine-grained amphibolite and pelitic rocks, in ascending order. **d**, A geological map of St. John's Harbour East area (SJHE). A supracrustal belt is composed of some fault-bounded blocks from ultramafic rocks through mafic rocks to sedimentary rocks of pelitic rocks, carbonate rocks and cherts in ascending order. The figures are modified from Figs 2, 3, 5 and 7 of Komiya *et al.*[8] with permission.

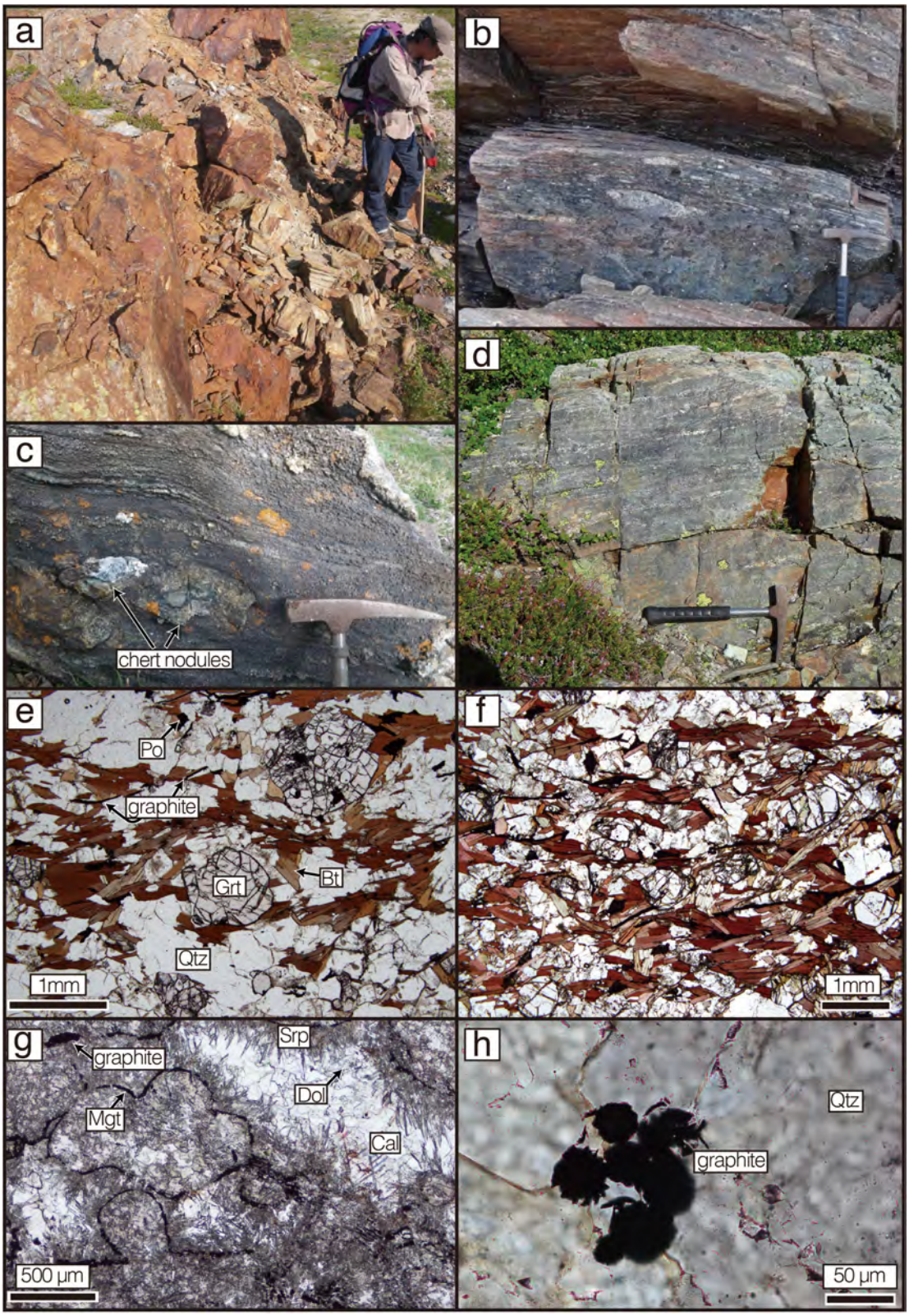

Extended Data Figure 2 | Photos of outcrops and thin sections of the metasedimentary rocks. a, An outcrop of pelitic rocks (LAA269, LAA270) at St. John's Harbour South. **b**, An outcrop of a conglomerate (LAD849A, LAD849B, LAD849C, LAD852) at St. John's Harbour East. The photo was taken from the east. A large siliceous clast in the conglomerate displays north to south extension. **c**, A carbonate rock (LAA742) with chert nodules at St John's Harbour East. **d**, An outcrop of the chert at St. John's Harbour East. **e**, A representative microscopic image of a pelitic rock (LAF492), containing biotite (Bt), garnet (Grt), quartz (Qtz), pyrrhotite (Po) and graphite. The most graphite grains have elongated shapes and occur along biotite grains and within garnet grains. **f**, Another representative microscopic image of a pelitic rock (LAF491). The graphite occurs along the biotite grains, forming bedding planes, or along the cleavages of the biotites. **g**, A microscopic image of a carbonate rock (LAA766). The needle-like mineral is serpentine (Srp), and sparry carbonate consists of calcite (Cal) and dolomite (Dol). Magnetite (Mgt)-rich rings are present in the fine-grained carbonate (Cal). **h**, A microscopic image of a chert nodule (LAA760) in the carbonate rock (**c**). The graphite grains have globular shapes, and form an aggregate.

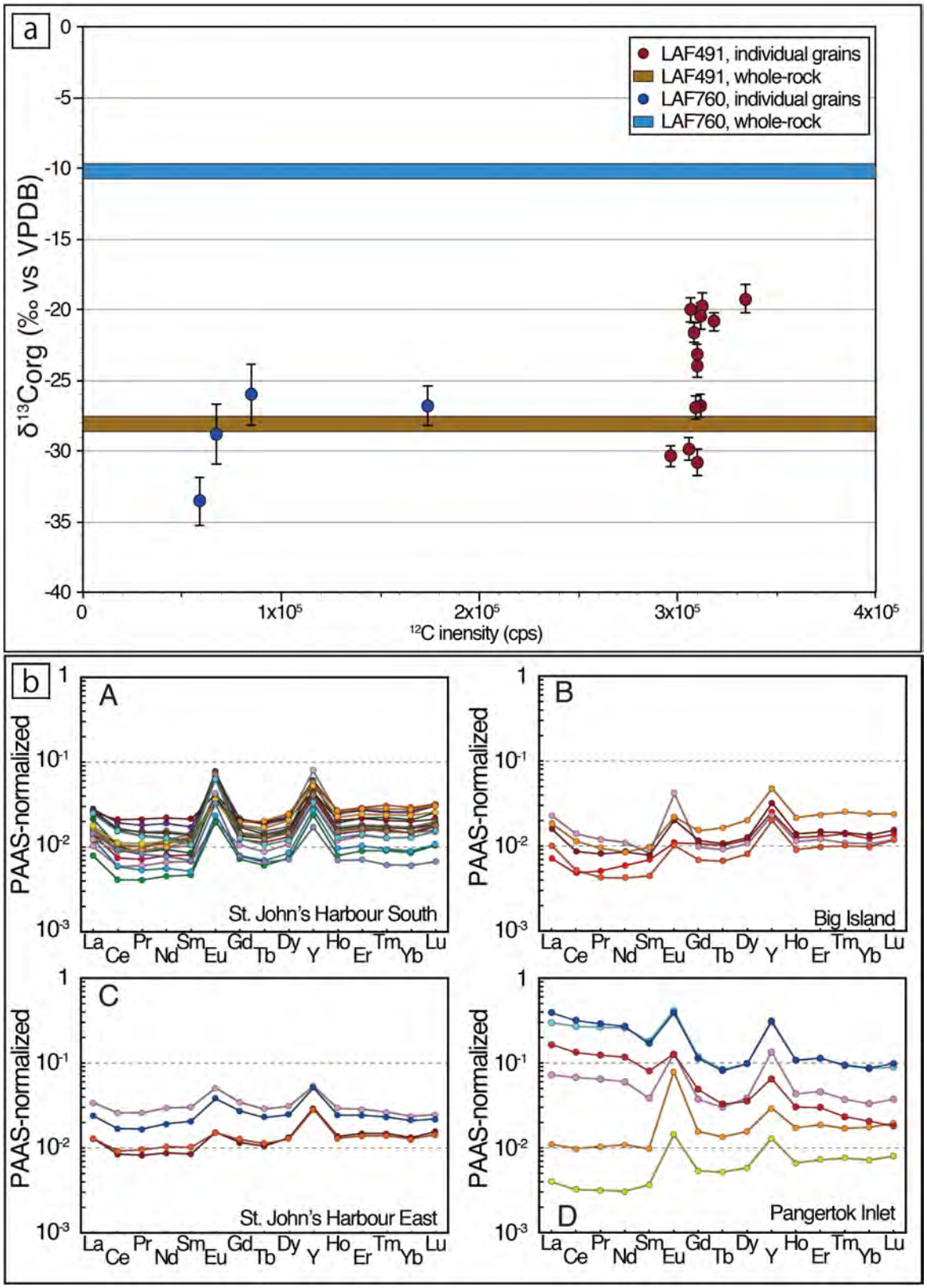

Extended Data Figure 3 | Carbon isotope values of individual graphite grains and rare earth element+Y patterns of carbonate rocks. a, Carbon isotope values of individual graphite grains in a pelitic rock (LAF491) and a chert nodule of carbonate rock (LAA760). The graphite grains in the LAF491 range from −19.3 to −30.8‰ in $\delta^{13}C_{org}$ values, whereas those in the LAA760 vary from −26.1 to 33.6‰ in $\delta^{13}C_{org}$ values. The formers are consistent with the whole-rock carbon isotope ratio (−28.2‰) but the latter is much lower than the whole-rock value (−10.3‰). **b**, Post-Archean-Australian-shale-normalized rare earth element + Y diagrams of carbonate rocks with low Y and Zr contents. The carbonate rocks show diagnostic Eu and Y anomalies in the St. John's Harbour South (A), Big Island (B), St. John's Harbour East (C), and Pangertok Inlet (D).

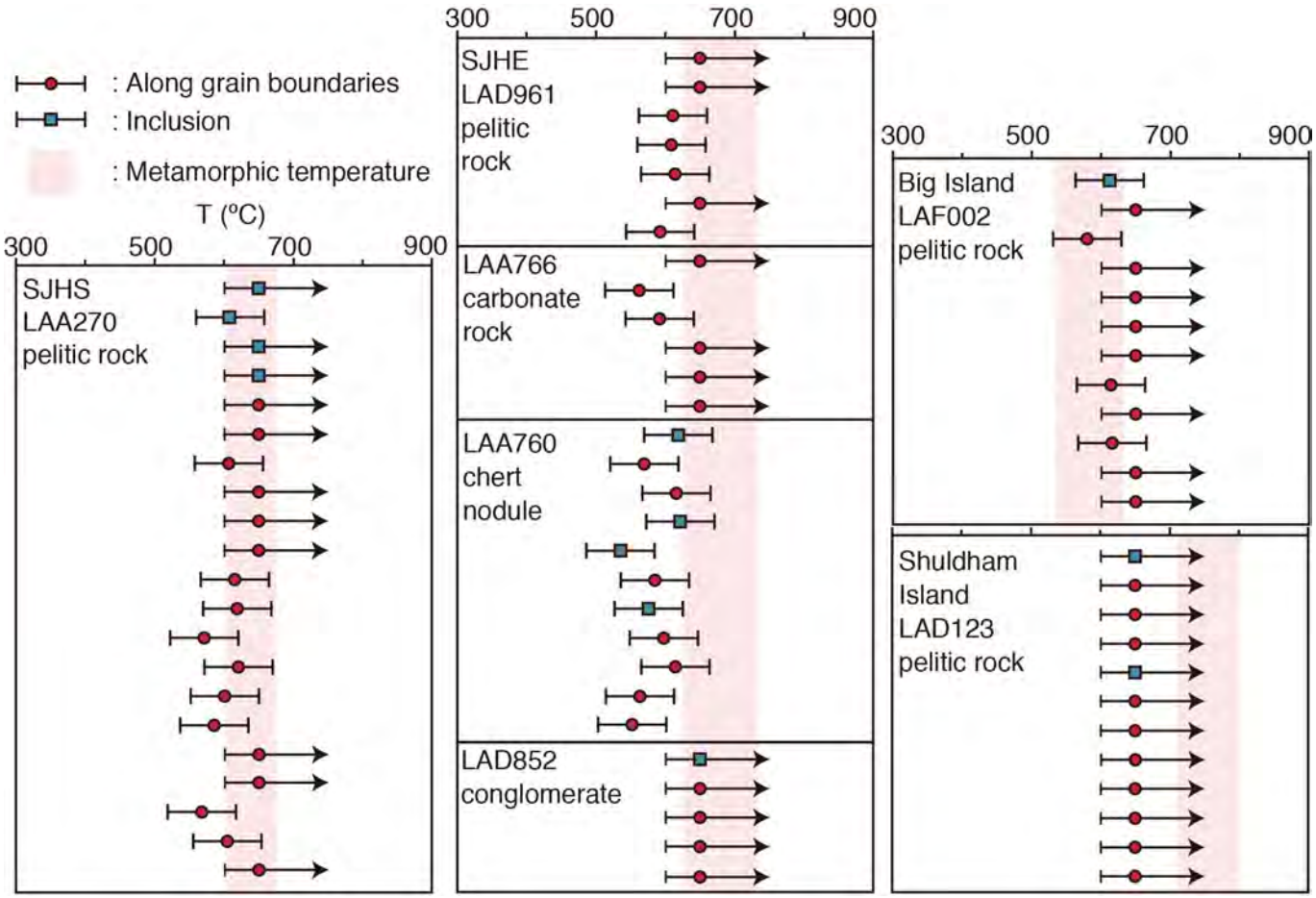

Extended Data Figure 4 | The comparison between metamorphic temperature and crystallization temperature of graphite. The metamorphic temperatures were estimated from mineral parageneses of metabasaltic rocks and compositions of garnet and biotite in pelitic rocks, whereas the crystallization temperatures were estimated from Raman spectra of graphite. In the case of absence of D1 bands, the estimated crystallization temperature is over 650 ± 50 °C. The estimated crystallization temperatures of graphite are consistent with the metamorphic temperatures except for those from a chert nodule.

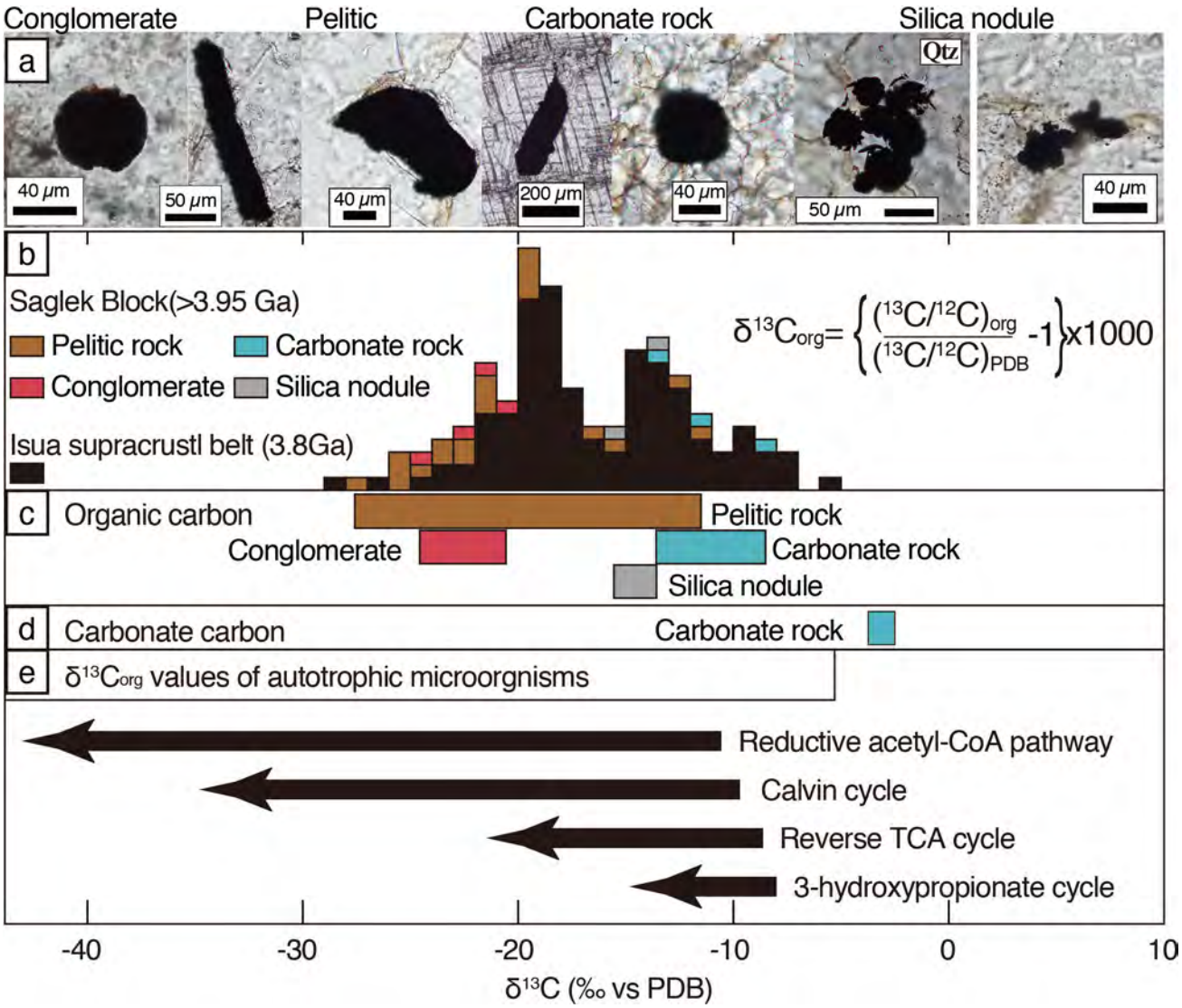

Extended Data Figure 5 | The distribution of the $\delta^{13}C_{org}$ values in Saglek Block and Isua supracrustal belt. The $\delta^{13}C_{org}$ values in Isua supracrustal belt range between −28 and −6‰[28–35]. The lower column shows variations of carbon isotope fractionation in four different carbon fixation pathways by modern autotrophic bacteria[36].

Extended Data Table 1 | Total organic carbon contents and carbon isotope values of graphite

Sample	Area	TOC (wt.%)	$\delta^{13}C_{org}$ (‰ vs VPDB)	$\delta^{13}C_{carb}$ (‰ vs VPDB)
Pelitic rock				
LAA269	SJHS	0.31	-19.9	
LAA270	SJHS	0.35	-25.6	
LAF487	SJHS	0.42	-22.2	
LAF489	SJHS	0.41	-26.2	
LAF490	SJHS	0.04	-24.9	
LAF491	SJHS	0.62	-28.2	
LAF492	SJHS	0.62	-22.7	
LAF493	SJHS	0.22	-20.9	
LAF494	SJHS	0.05	-27.4	
LAF495	SJHS	0.22	-21.8	
LAF497	SJHS	0.09	-23.7	
LAF498	SJHS	0.05	-17.3	
LAF500	SJHS	0.06	-24.2	
LAF002	Big Island	0.11	-18.1	
LAF005	Big Island	0.19	-18.6	
LAD961	SJHE	0.25	-16.6	
LAD983	SJHE	0.02	-21.1	
LAF645	SJHE	0.24	-14.9	
LAD123	Shuldham Island	0.12	-11.0	
LAF400	Shuldham Island	0.15	-12.9	
Conglomerate				
LAD849A	SJHE	0.07	-27.6	
LAD849B	SJHE	0.08	-20.8	
LAD849C	SJHE	0.07	-22.7	
LAD852	SJHE	0.06	-20.9	
Carbonate rock				
LAA766	SJHE	0.16	-6.9	
LAA767	SJHE	0.07	-9.9	
LAF647	SJHE	0.09	-8.2	
Chert nodule				
LAA760	SJHE	0.02	-10.3	
LAA763	SJHE	0.02	-9.9	
Carbonate rock				
LAA742	SJHE			-3.3
				-2.6
				-3.2
				-2.7
				-3.3
				-2.7
LAA766	SJHE			-3.5
				-3.4
				-3.5
				-3.6
				-3.5
				-3.3
				-3.4
LAA767	SJHE			-3.5
				-3.8
				-3.5
				-3.3

TOC: Total organic carbon contents

Extended Data Table 2 | Carbon isotope values of individual graphite grains

Sample	^{12}C intencity (cps)	$^{12}C^{2-}/^{12}C^{-}$	$^{12}C^{14}N^{-}/^{12}C$	$\delta^{13}C_{VPDB}$ (‰)	error (1σ)
LAF 491 graphite					
#1-1	3.07 x10^5	0.76	0.0031	-20.0	0.9
#1-2	3.12 x10^5	0.77	0.0024	-20.4	1.0
#2-1	3.09 x10^5	0.75	0.0023	-21.6	0.7
#2-2	3.18 x10^5	0.75	0.0023	-20.9	0.7
#3-1	3.09 x10^5	0.61	0.0035	-27.0	0.8
#3-2	3.11 x10^5	0.58	0.0061	-26.8	0.8
#4-1	3.13 x10^5	0.65	0.0025	-19.7	0.9
#5-1	3.34 x10^5	0.55	0.0036	-19.3	1.0
#5-2	3.10 x10^5	0.55	0.0029	-30.8	0.9
#6-1	2.96 x10^5	0.63	0.0021	-30.4	0.8
#6-2	3.05 x10^5	0.54	0.0027	-29.9	0.8
#7-1	3.10 x10^5	0.58	0.0029	-24.1	0.7
#8-1	3.10 x10^5	0.66	0.0027	-23.2	0.7
LAA 760 graphite					
#1-1	1.74 x10^5	0.81	0.1884	-26.8	1.4
#3-1	6.77 x10^5	0.82	0.0833	-28.9	2.1
#5-2	8.46 x10^5	0.78	0.1402	-26.1	2.1
#6-1	5.87 x10^5	0.61	0.2596	-33.6	1.7

Extended Data Table 3 | Representative compositions of garnet and biotite

	garnet					biotite			
	LAA492 rim	LAD961 rim	LAF002 rim	LAD123 rim	LAD123 core	LAA492	LAD961	LAF002	LAD123
SiO_2	37.8	37.5	38.1	38.6	38.7	34.3	34.6	36.5	38.2
TiO_2	-	0.02	0.04	0.02	-	1.90	3.24	2.45	1.47
Al_2O_3	20.5	21.9	21.3	21.7	22.1	18.3	18.2	17.6	18.3
Cr_2O_3	0.03	0.06	0.11	0.15	0.15	0.12	0.20	0.32	0.35
FeO^{tot}	34.0	33.6	30.9	27.0	26.2	20.4	16.8	12.8	9.2
MnO	2.10	1.27	1.64	1.18	1.16	0.02	0.00	0.03	0.02
MgO	3.58	5.37	6.51	8.61	10.0	9.74	11.3	14.7	18.2
CaO	2.23	1.14	1.56	2.59	2.71	0.02	-	-	0.02
Na_2O	-	0.01	-	-	0.04	0.04	0.24	0.18	0.18
K_2O	0.02	0.02	0.04	-	0.03	9.86	10.1	10.5	9.82
Total	100.14	100.77	100.08	99.72	100.98	94.64	94.53	94.73	95.44

Total iron as FeO

Extended Data Table 4 | Summary of Raman spectrum parameters of graphite and estimated temperatures

Sample	G center	G FWHM	G area	D1 area	D2 area	R2 (D1/(G+D1+D2) area ratio)	Estimated temperature (°C)	Occurrence
LAA270-1	1580	16	8.47	-	-	-	-	in Grt
LAA270-2	1582	16	4.61	0.38	0.08	0.08	607	in Grt
LAA270-3	1580	17	8.90	-	-	-	-	in Grt
LAA270-4	1579	17	46.69	-	-	-	-	in Qtz
LAA270-5	1580	18	28.39	3.92	1.61	0.12	590	Qtz-Qtz boundary
LAA270-6	1580	17	35.33	-	-	-	-	Qtz-Pl boundary
LAA270-7	1581	15	17.65	1.49	0.09	0.08	607	Qtz-Pl boundary
LAA270-8	1580	18	4.03	-	-	-	-	Qtz-Qtz boundary
LAA270-9	1580	14	7.59	-	-	-	-	Qtz-Bt-Grt boundary
LAA270-10	1581	17	5.75	-	-	-	-	Qtz-Bt boundary
LAA270-11	1582	18	60.83	3.81	2.42	0.06	616	Qtz-Bt boundary
LAA270-12	1582	18	12.01	0.62	0.04	0.05	619	Qtz-Bt boundary
LAA270-13	1581	21	38.09	8.34	6.81	0.16	571	Qtz-Bt boundary
LAA270-14	1581	14	24.82	1.20	0.19	0.05	621	Qtz-Bt boundary
LAA270-15	1580	16	20.27	2.18	2.06	0.09	601	Qtz-Qtz boundary
LAA270-16	1581	18	33.96	5.02	1.49	0.12	586	Qtz-Bt boundary
LAA270-17	1581	19	22.18	-	-	-	-	Qtz-Bt boundary
LAA270-18	1583	16	54.84	-	-	-	-	Qtz-Bt boundary
LAA270-19	1582	18	36.31	7.41	1.58	0.16	568	Qtz-Bt boundary
LAA270-20	1581	18	43.63	4.03	2.09	0.08	605	Qtz-Bt boundary
LAA270-21	1579	17	18.18	-	-	-	-	Qtz-Pl-Po boundary
LAA270-22	1581	15	7.79	-	-	-	-	Qtz-Qtz boundary
LAD123-1	1578	15	42.77	-	-	-	-	in Qtz
LAD123-2	1580	16	6.92	-	-	-	-	Qtz-Amp boundary
LAD123-3	1578	15	39.72	-	-	-	-	Qtz-Qtz boundary
LAD123-4	1579	15	37.33	-	-	-	-	Pl-Bt boundary
LAD123-5	1578	17	25.41	-	-	-	-	in Qtz
LAD123-6	1578	15	36.21	-	-	-	-	Qtz-Pl boundary
LAD123-7	1579	14	17.46	-	-	-	-	Qtz-Pl boundary
LAD123-8	1579	15	20.57	-	-	-	-	Qtz-Pl boundary
LAD123-9	1580	14	9.43	-	-	-	-	Qtz-Bt boundary
LAD123-10	1582	18	29.83	-	-	-	-	Qtz-Pl boundary
LAD123-11	1580	14	22.58	-	-	-	-	Qtz-Bt boundary
LAD123-12	1580	15	21.26	-	-	-	-	Qtz-Qtz boundary
LAD961-1	1578	18	37.73	-	-	-	-	Qtz-Qtz boundary
LAD961-2	1579	15	13.39	-	-	-	-	Qtz-Bt boundary
LAD961-3	1579	18	25.41	2.10	3.67	0.07	611	Qtz-Bt boundary
LAD961-4	1578	16	8.84	0.69	0.08	0.07	609	Pl-Bt boundary
LAD961-5	1577	19	32.12	2.04	0.19	0.06	615	Qtz-Bt boundary
LAD961-6	1578	14	23.81	-	-	-	-	Qtz-Pl-Bt boundary
LAD961-7	1581	20	25.37	3.45	3.35	0.11	593	Pl-Pl boundary
LAF002-1	1582	19	14.69	1.03	0.48	0.06	613	in Qtz
LAF002-2	1579	16	16.88	-	-	-	-	Qtz-Bt boundary
LAF002-3	1580	18	19.84	3.26	0.82	0.14	580	Pl-Bt boundary
LAF002-4	1582	19	14.56	-	-	-	-	Pl-Pl boundary
LAF002-5	1580	16	17.35	-	-	-	-	Qtz-Pl-Bt boundary
LAF002-6	1581	15	12.86	-	-	-	-	Qtz-Bt boundary
LAF002-7	1581	19	7.29	-	-	-	-	Bt-Bt boundary
LAF002-8	1581	20	13.22	0.83	0.00	0.06	615	Qtz-Bt boundary
LAF002-9	1582	17	22.36	-	-	-	-	Pl-Bt boundary
LAF002-10	1581	18	5.51	0.34	0.27	0.05	617	Bt-Bt boundary
LAF002-11	1580	15	6.81	-	-	-	-	Qtz-Pl-Bt boundary
LAF002-12	1579	16	15.15	-	-	-	-	Qtz-Bt boundary
LAD852-1	1579	15	7.58	-	-	-	-	in Pl
LAD852-2	1582	16	4.31	-	-	-	-	Qtz-Pl boundary
LAD852-3	1579	15	4.24	-	-	-	-	Pl-Bt boundary
LAD852-4	1581	16	5.47	-	-	-	-	Qtz-Pl boundary
LAD852-5	1581	19	5.91	-	-	-	-	Qtz-Pl boundary
LAA766-1	1582	14	5.20	-	-	-	-	Cbn-Cbn boundary
LAA766-2	1580	15	21.52	5.05	2.09	0.18	563	Cbn-Srp boundary
LAA766-3	1580	18	11.40	1.58	1.47	0.11	592	Cbn-Srp boundary
LAA766-4	1581	16	23.90	-	-	-	-	Cbn-Cbn boundary
LAA766-5	1580	19	9.55	-	-	-	-	Cbn-Cbn boundary
LAA766-6	1581	17	38.30	-	-	-	-	Cbn-Cbn boundary
LAA760-1	1581	19	16.67	0.88	0.11	0.05	619	in Qtz
LAA760-2	1582	21	20.13	3.89	0.13	0.16	569	Qtz-Qtz boundary
LAA760-3	1581	20	17.59	1.07	0.54	0.06	616	Qtz-Qtz boundary
LAA760-4	1581	17	20.27	0.92	0.18	0.04	622	in Qtz
LAA760-5	1581	18	8.83	2.86	0.36	0.24	536	in Qtz
LAA760-6	1581	19	6.71	0.96	0.12	0.12	586	Qtz-Qtz boundary
LAA760-7	1581	19	5.18	0.94	0.33	0.15	576	in Qtz
LAA760-8	1582	21	13.03	1.38	0.07	0.10	599	Qtz-Qtz boundary
LAA760-9	1581	18	21.86	1.39	0.04	0.06	614	Qtz-Qtz boundary
LAA760-10	1582	19	8.64	1.98	0.69	0.18	563	Qtz-Qtz boundary
LAA760-11	1581	18	22.66	5.72	0.51	0.20	553	Qtz-Qtz boundary